# Effect of Prosthetic Knee Stiffness on the Sit-to-Stand Movement of a Unilateral Transfemoral Amputee Model

## A Predictive Simulation Study

Master Thesis

Yimeng Li

Delft University of Technology

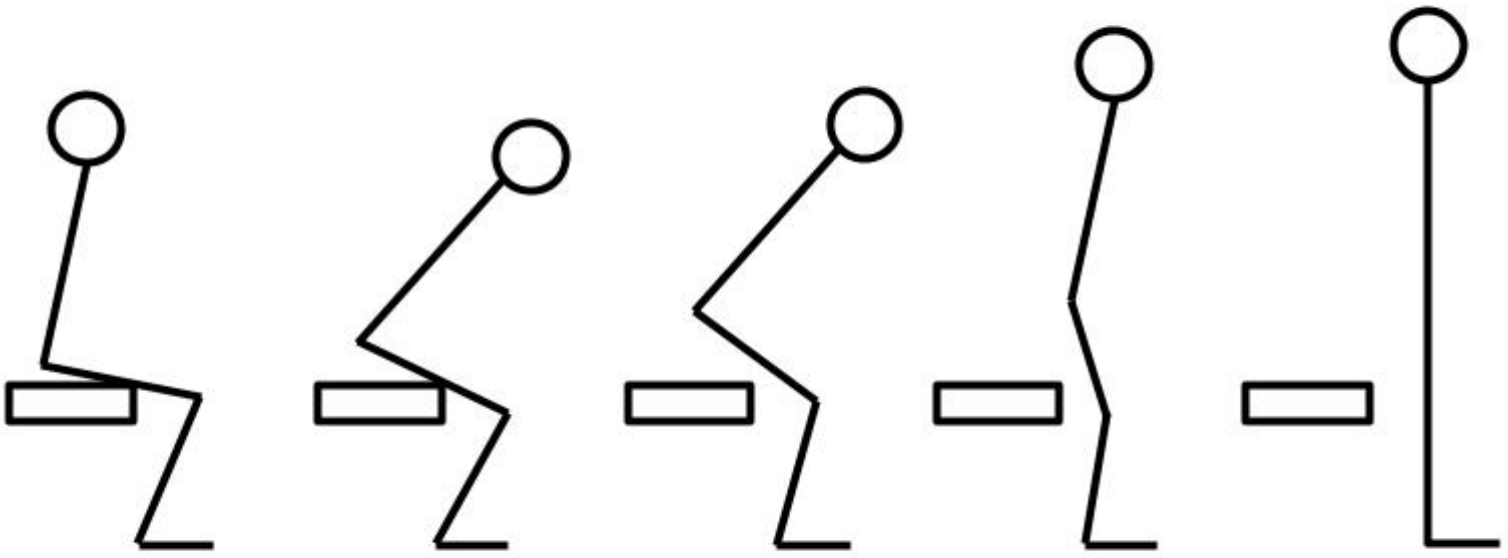

# Effect of Prosthetic Knee Stiffness on the Sit-to-Stand Movement of a Unilateral Transfemoral Amputee Model

## A Predictive Simulation Study

by

Yimeng Li

to obtain the degree of Master of Science

at Delft University of Technology,

to be defended publicly on Thursday July 11, 2024 at 10:00 AM.


| | | |
|---|---|---|
| Student number: | 5306469 | |
| Project duration: | October, 2023 – July, 2024 | |
| Thesis committee: | Prof. Dr. Ing. Heike Vallery, | TU Delft, Supervisor |
| | Dr. Ir. Gerwin Smit, | TU Delft, Supervisor, Chairman |
| | Ir. Bob van der Windt, | TU Delft, Supervisor |
| | Dr. Ir. Ajay Seth, | TU Delft |




TU Delft

# Acknowledgements

I am deeply grateful to my supervisors, Prof. Dr. Ing. Heike Vallery, Dr. Ir. Gerwin Smit, and their Ph.D. student Ir. Bob van der Windt, for providing me the opportunity to work on this project and for their invaluable guidance and support throughout the research.

My heartfelt thanks go to Heike, whose meticulous attitude has profoundly influenced my approach to research and academic work. I hope to carry this meticulous attitude into my future work as well. Her ingenuity has also enlightened me throughout the research process.

I extend my sincere appreciation to Gerwin, who has imparted research methodologies and knowledge to me in an interesting and engaging manner, often using apt analogies to make complex concepts more understandable. He is very dedicated to his students and always goes the extra mile to ensure we succeed. The bi-weekly meetings were something I truly enjoyed.

Special thanks are to my daily supervisor, Bob, for his continuous encouragement and enthusiasm. Modeling and coding are not my strong suits, but his enthusiasm and positive feedback gave me the courage and confidence to complete my work. Without his support, I would not have been able to finish my thesis.

I am also thankful to Dr. Ir. Ajay Seth, Dr. Ir. Eline van der Kruk, and Dr. Adam Kewley for their consultation and advice on the topic. Special gratitude goes to Dr. Thomas Geijtenbeek for his invaluable assistance with the SCONE and Hyfydy software. He has been very kind and patient in answering questions about SCONE and Hyfydy. His expertise and support were crucial in the successful implementation of my simulations. Their generosity with their time and knowledge is greatly appreciated.

Finally, I extend my heartfelt thanks to my parents, friends, and fellow students for their unwavering support, understanding, and companionship. Special thanks go to my parents for respecting my choices and always supporting and understanding me. Their encouragement has been vital to my perseverance and success in this journey.

It has also been my pleasure to meet so many wonderful people here.

*Sincerely,*
*Yimeng Li*
*Delft, June 2024*

# Table of Contents

CONTENTS

# Effect of Prosthetic Knee Stiffness on the Sit-to-Stand Movement of a Unilateral Transfemoral Amputee Model – A Predictive Simulation Study

Yimeng Li

***Abstract*—Optimal settings and designs for prosthetic parameters, such as knee stiffness, are required to achieve effective and stable sit-to-stand (STS) movements for individuals with lower limb prostheses but remain inadequately defined. One possible solution is prosthetic modeling and predictive simulations. However, current literature primarily focuses on inverse kinematics, inverse dynamics, and most likely, gait. There remains a gap in optimizing the parameters during STS movement through predictive simulation. By utilizing SCONE (Simulated Controller OptimizatioN Environment for predictive simulating), this study aims to find the optimized prosthetic parameters and investigate the effect of varying transfemoral prosthetic knee joint stiffness on biomechanics and validate this approach. A modified musculoskeletal model with a prosthesis and neuromuscular controllers are combined for predictive sit-to-stand simulation. The control parameters for neuromuscular controllers and the prosthetic parameters are optimized by SCONE with predefined objective functions to obtain energy-oriented results. The simulation results were analyzed in terms of joint load, stability, kinematics, and energy cost. Lastly, the results were validated by comparison with an existing experimental dataset.The simulations indicated that prosthetic knee stiffness affects joint loads, stability, kinematics, and energy expenditure during STS movements. Higher knee stiffness generally leads to increased prosthetic side joint loads and contribution but requires higher damping ratios to ensure a successful STS movement, while extreme stiffness should be avoided. Optimal stiffness settings were identified near $70\,\mathrm{N\,m\,rad^{-1}}$ with the damping ratio of $22\,\mathrm{N\,m\,s\,rad^{-1}}$. Validation shows the feasibility of this approach as well as its limitations. This study demonstrates the potential and insights of predictive simulations in optimizing prosthetic knee parameters. However, the current approach is limited by the model, methodological, theoretical, and practical issues. Therefore, further validation and refinement are necessary. Future work may focus on building complex and customized models and exploring other movements.***

## I. Introduction

### A. Background

Rising from a chair is a common activity of daily living [1]. The ability to perform sit-to-stand (STS) movements independently and efficiently is critical for individuals with lower limb prostheses [2], as it impacts their mobility and quality of life [3]. The prosthetic knee joint and ankle joint play important roles in these movements [4], particularly for transfemoral amputees, who rely on the functionality [5], [6] and stability [7] provided by their prosthetic limbs.

Prosthetic design [8] and exoskeleton technology [9] have advanced significantly, with the integration of actuators that enhance mobility through passive and active mechanisms [6]. These advancements aim to mimic the natural movement of the human knee [10], thereby improving the overall functionality of prosthetic limbs. However, the optimal stiffness or damping ratio settings for these prostheses during STS movements remain a critical area of research, as inappropriate stiffness can lead to increased joint loads on the intact leg, potentially elevating the risk of falls and other complications.

### B. Problem Statement

Despite significant advancements, optimal design characteristics and parameters such as prosthetic joint stiffness and damping ratio are not well-addressed, as their influence on biomechanical factors (e.g., metabolic cost and joint loading) remains unclear [11]. Price et al. also noted the lack of exploration regarding the effects of prosthetic joints on whole-body biomechanics and user experience [12]. This problem of finding optimal prosthetic design and parameters directly impacts prosthetic users, who rely on these devices for daily mobility. Additionally, it affects researchers and designers working to innovate and improve prosthetic technologies, as well as orthotists and prosthetists who are responsible for fitting and adjusting prosthetic devices to meet individual needs.

Modeling and simulation offer a potential solution to this problem. These simulations can model and analyze various scenarios to identify the optimal settings for prosthetic parameters [13]. By utilizing simulations, it is possible to minimize the trial-and-error process traditionally used in prosthetic adjustments, leading to more effective, goal-directed, and movement-specific tuning of prosthetic devices. However, existing prosthetic models and simulations typically focus on simulating inverse kinematics [14], inverse dynamics [15], and mostly gait tasks [11], [16]–[18], without adequately addressing the requirements of STS movements for prosthetic users.

This report addresses the challenge of optimizing prosthetic knee and ankle parameters to facilitate efficient and stable STS movements. There is a need for more adjustable prosthetic models and simulation configurations that can systematically and specifically optimize these actuator parameters, ensuring better load distribution, stability, and energy efficiency.

### C. Objective

The objective of this thesis is, through predictive simulation and prosthetic modeling, to find the optimized prosthetic parameters and to investigate the effect of varying the transfemoral prosthetic knee joint stiffness on the biomechanics of sit-to-stand movements. Identifying optimal prosthetic knee stiffness options by assessing joint load, stability, kinematics, and energy efficiency during sit-to-stand movement. Validation

is performed by comparing with the existing experimental kinematic data. By achieving these objectives, this study aims to contribute to the predictive simulation of designing more effective and stable prosthetic knee and ankle joints, ultimately improving the STS movement of lower limb prostheses by way of parameter optimization.

## II. Materials and Methods

A musculoskeletal model with prosthesis and neuromuscular controllers is combined for predictive sit-to-stand simulation, where the control parameters for neuromuscular controllers and the prosthetic parameters are optimized using a shooting-based optimization method. The results are analyzed and evaluated in terms of joint load, stability, and energy cost, additionally, are compared with an existing experimental dataset of recorded kinematics.

### A. Softwares

*1) OpenSim:* An open-source software enables the users to model neuromusculoskeletal systems, conduct forward and backward simulations, and analyze the respective results of both experiments and simulations [19]. The OpenSim Application Programming Interface (API) allows further exploration of novel models and algorithms which are not currently supported by OpenSim such as OpenSim Musculoskeletal optimal control (MOCO) [20].

*2) SCONE:* Simulated Controller OptimizatioN Environment (SCONE) is a free and open-source software designed for predictive simulations of neuromusculoskeletal system motion. SCONE uses a shooting-based optimizer to optimize the parameters of controllers or the neuromusculoskeletal model so that the model can perform a specific task and achieve the optimization objectives [21]. Specifically, based on control algorithms and weighted cost functions, SCONE can conduct predictive simulations and optimize the movement of the task using the Covariance Matrix Adaptation Evolution Strategy (CMA-ES).

The model can be either the OpenSim model (.osim file) or the Hyfydy model (.hfd file), which can be converted from the OpenSim model. Hyfydy is a plug-in for SCONE that serves as a new simulation engine for accurate, high-performance biomechanical simulations by using explicit forces to handle constraints and combining this with a novel error-controlled integrator [22].

An elementary controller computes the input values of the model actuators, which are muscles in most cases. Generally, they are feed-forward controllers and feedback controllers. Feed-forward controllers generate fixed patterns based on a parameterized function, while feedback controllers generate actuator inputs based on sensor information. SCONE provides various modular and predefined controllers that can be combined to create complex behaviors for complicated systems, such as STS and sit-to-walk (STW).

Objective functions in SCONE are called measures, which return a score indicating how well the movement task is performed according to the research interests. The goal of the predictive simulation is to find the optimal motion for a specific task, which is described by the objective functions and controllers.

*3) OpenSim Creator:* This is a standalone and open-source UI for building and editing OpenSim models, as well as conducting simulations [23]. It enables users to visually build and edit OpenSim models, such as adding constraints and joints, to empower model development for biomechanical research.

### B. Modeling and Controller

*1) Model:* Two musculoskeletal models are referred to in this thesis. The first model serves as a reference and guidance to provide muscle autonomy information after amputation. This OpenSim model represents individuals with an osseointegrated unilateral transfemoral amputation with a generic prosthesis [16]. This model was modified based on Gait2392 to have 19 degrees of freedom (DOFs) and 76 musculotendon units. Due to the transfemoral amputation, partial muscles on the prosthetic side are removed, and eight bi-articular muscles (i.e., semimembranosus, semitendinosus, biceps femoris long head, sartorius, adductor magnus, tensor fascia latae, gracilis, and rectus femoris) are re-attached and anchored to the transected femur bone. According to Raveendranathan et al. [16], these eight muscles are disabled during simulations due to the lack of clinical evidence of their contribution to the movement in the literature.

The second model is an STW model developed by van der Kruk and Geijtenbeek [24]. This Hyfydy model represents a male adult with a height of $1.80\,\mathrm{m}$ and a mass of $75\,\mathrm{kg}$ with a box chair [24]. It was developed based on a musculoskeletal model (H1120) with 11 degrees of freedom and 20 Hill-type muscle-tendon units. A reduction in the number of muscles was conducted by combining muscles with similar functions in the sagittal plane into single units with combined peak isometric force to represent 11 major bilateral muscle groups.

The prosthetic user model, shown in Figure 1, is modified based on the STW model (second model) for this predictive simulation. The right leg was selected to represent the prosthetic leg, which can be found in Figure 2. Firstly, the tibant, soleus, gastroc, vasti, and bifemsh muscles of the right side are removed to mimic the amputation. The biarticular hamstrings and rectus femoris muscles are reattached to the point where the femur is assumed to be amputated by referring to the first model. Therefore, the muscles' path, attachment points, and tendon slack length in the Hyfydy model are adjusted. It should be noted that the effect of amputation on the reattached muscles and the effect on the socket is not the focus of this thesis. The mass property and inertial property of the prosthetic side are not changed, which means the prosthesis is assumed to have the same mass and inertia as the intact leg. The reason is that it is better to overestimate the mass than to underestimate it.

The prosthetic knee joint and ankle are passive devices with a certain stiffness and damping ratio in this model. As shown in Figure 2, the right-side knee and ankle are replaced by passive devices, each with its own set of stiffness and damping ratios independently. In the Hyfydy model, the prosthetic knee

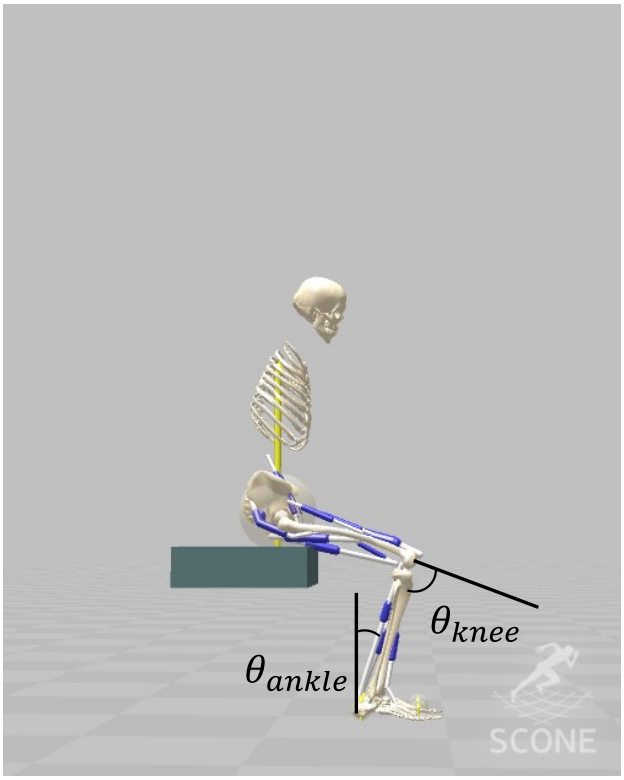


Fig. 1: The modified musculoskeletal model(Hyfydy model file based on H1120) has 11 degrees of freedom and is actuated using 15 Hill-type muscle-tendon units with 4 joint motor actuators. Each body frame is shown in this figure and is located at its corresponding body COM. The grey box behind the model represents the contact model of the chair

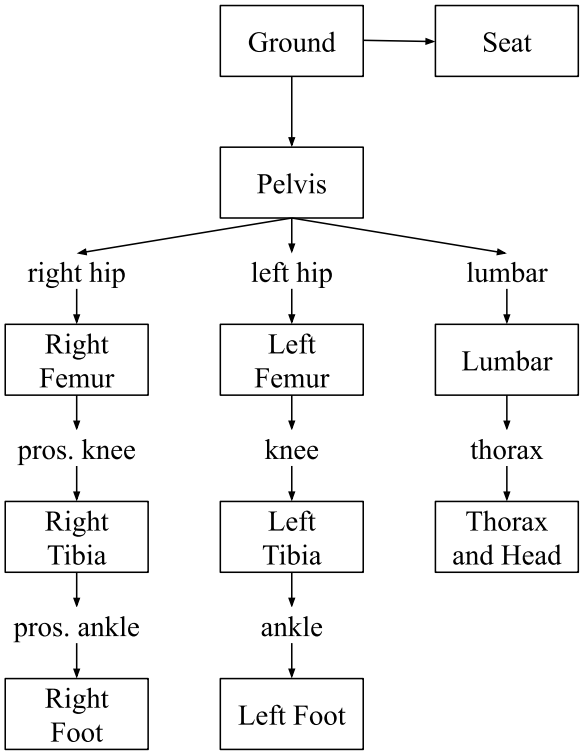


Fig. 2: Topology diagram illustrating the various bodies and joints within the prosthetic model, where bodies are represented as boxes and joints are represented separately and are not enclosed within the boxes. It shows that the right knee joint and ankle joint are replaced by a prosthetic knee and prosthetic ankle (pros. knee and pros. ankle).

joint, prosthetic ankle joint, lumbar joint, and thoracic joint are represented by 'joint motor' actuators [22]. These joint motors can produce joint torque based on the joint angle and joint velocity:

$$\tau = k_p \left(q - q_t\right) + k_d \left(\omega_t - \omega\right), \tag{1}$$

where the amount of output $\tau$ is a function of the stiffness $k_p$ (optimized by SCONE), damping ratio $k_d$ (optimized by SCONE), orientation $q$ (joint angles), target orientation $q_t$ (predefined joint angles, which are $0\,\mathrm{rad}$), angular velocity $\omega$ (joint angular velocities), and target angular velocity $\omega_t$ (predefined joint angular velocities, which are $0\,\mathrm{rad\,s^{-1}}$). The maximum and minimum torque output of the joint motor is between $[-\tau_{max}, \tau_{max}]$.

The Hunt-Crossley model [25] is used to define the contact forces between the buttocks and the chair and between the feet and the ground. Specifically, the pelvis is defined by one contact sphere of 12 cm to represent the buttocks. The chair is a box with dimensions of $40\,\mathrm{cm} \times 12\,\mathrm{cm} \times 5\,\mathrm{cm}$. Two contact spheres with a radius of 3 cm are located at the heel and toes of each foot. The contact spheres at the feet have a plane strain modulus of $17\,500\,\mathrm{N/m^2}$ and at the chair $10\,000\,\mathrm{N/m^2}$. The dissipation coefficient, static friction, and dynamic friction coefficients of all contact spheres are $1\,\mathrm{s\,m^{-1}}$, 0.9, and 0.6 respectively. There are also joint limit stiffness and dampers to represent the ligaments.

The muscle force model m2012fast is adopted in the STS Hyfydy model [22]. This is an optimized version of the Hill-type muscle developed by Millard et al. [26], including a passive damping term that allows velocity to be determined even when the muscle is deactivated. There are some major differences in the implementation of the Millard Equilibrium Muscle between the Hyfydy and OpenSim. Firstly, the curves of force-length and force-velocity relationships for passive tendon and muscle forces in Hyfydy are described by polynomials instead of splines, which leads to differences between Hyfydy results and OpenSim results. Secondly, the muscle damping forces are computed by an explicit method instead of using an iterative method as in OpenSim, which is suggested in the literature.

*2) Controllers:* Three reflex controllers are combined together as a consequential controller in SCONE to control the STS movement for different phases of the STS. This adjustment is based on the original STW model simulation, which adopted a consequential controller consisting of two reflex controllers and a gait controller. For STS simulations, since there is no gait movement involved during sit-to-stand, the gait controller is replaced by another reflex controller to control the quiet standing state for balance control.

Each reflex controller contains its own set of control parameters. Monosynaptic and antagonistic proprioceptive feedback from the muscles and vestibular feedback related to the pelvis tilt are integrated to construct the reflex controller [24]. The general equation for the proprioceptive control is:

$$\begin{aligned} U = C_0 + K_L(L(t-\delta_t)) - L_0 \\ + K_F(F(t-\delta_t)) + K_V(V(t-\delta_t)) \end{aligned} \tag{2}$$

where $K_L$, $K_F$, and $K_V$ are the gains of the controller, $C_0$ is the constant base actuation, and $L_0$ is the length offset, which is set to 1. $L(t)$ is the normalized CE length $(L/L_{opt})$ at time $t$. $K_L$, $K_F$, $K_V$, and $C_0$ are to be optimized by SCONE. However, $L_0$ is not optimized to distinguish it from $C_0$, where $(K_L L_0)$ is also a constant actuation. Lastly, the lumbar joint motor and thoracic joint motor in the Hyfydy model are controlled by a PD control based on the velocity and position of the respective joints.

Neural latencies in monosynaptic, antagonistic, and vestibular feedback were included as multiples of $5\,\mathrm{ms}$ according to [24]. The latencies of each part are not changed in the prosthetic model.

Overall, 537 free parameters are optimized. Apart from the controllers' parameters, the prosthetic knee and ankle joint stiffness and damping ratio are also optimized. In addition, those controllers that aim to control the deleted muscles or require feedback from the deleted muscles are removed from the controllers' list.

### C. Simulation and Optimization Flow

*1) Simulation and Optimization:* The optimization of the parameters, equations of motion, and the related integration were conducted by SCONE. All the simulations started with the same initial sit position with fixed joint angles and zero initial velocities, identical to the normal sit position in the STW model simulations [24]. Simulations stopped when the model fell or when the maximum simulation time ($15\,\mathrm{s}$) was reached. A fall event that terminates the simulation was defined as the COM height falling below 0.6 times its initial height at the beginning of the simulation.

The prosthetic knee joint stiffness was systematically varied across 10 predefined settings, from $0\,\mathrm{N\,m\,rad^{-1}}$ to $90\,\mathrm{N\,m\,rad^{-1}}$ with an increment of $10\,\mathrm{N\,m\,rad^{-1}}$. However, the prosthetic knee damping ratio, prosthetic ankle stiffness, and prosthetic ankle damping ratio were not varied. Therefore, 10 sets of simulations were conducted. For each set, multiple optimizations with the same configurations were conducted simultaneously to find the best local optimum. The optimization results for analysis were chosen according to the best fitness. All the parameters were optimized according to the optimization objectives by minimizing the weighted summation of all the measure terms. Measure terms contribute to a high-level and specific description of a movement, which is the STS task in this thesis.

*2) Objective Functions and Measures:* Height measure: For STS movement, one of the most important objectives for this task is to achieve a certain height and remain standing until the end of the simulation. During the simulation, the height measure was defined by the COM height reaching a height of $0.9\,\mathrm{m}$ and below $1.1\,\mathrm{m}$ to prevent jumping movement. The start and end times of this height measure were not defined, but a threshold was set to compensate for the penalty during standing up before the COM reaches $0.9\,\mathrm{m}$. This measure becomes zero if it is below the given threshold.

Joint angle measure: Apart from the height measure, the lumbar joint angle, thorax joint angle, pelvis tilt angle, and the lower extremities (hip, knee, and ankle joint angles) were limited to a certain range to penalize excessive joint angles and prevent unreasonable postures during STS movement. Only the measure of pelvis tilt had a threshold, and only the measures of the lower extremities had a start time ($1.5\,\mathrm{s}$) to start penalizing these hip, knee, and ankle joints after reaching the standing position.

GRF measure: An additional GRF measure was included in the simulation to ensure that the loading was not concentrated on one of the legs, especially to prevent single-leg tasks where the intact leg contributes most to the STS movement.

Head acceleration: A head acceleration penalty was set to prevent fast ascending and descending during the stand-up phase. The boundary was set to be $1\,\mathrm{m\,s^{-2}}$; if the magnitude of the head acceleration is within this interval, the measure returns zero.

Energy measure: Lastly, two measures were included to measure the energy cost during the STS movement. First, metabolic energy expenditure [27] calculated the overall energy cost during the STS movement. Secondly, a measure of the cubed muscle activation was applied to minimize the overall muscle activation. Additionally, the cubed muscle stress term was multiplied by 100 during the optimization to make it comparable with the metabolic energy term. These two measures were the major terms that contributed to the final objective function.

### D. Metrics

The evaluation of the simulation results of this thesis focuses on three aspects of the kinematic and kinetic datasets: joint loading, stability metrics, and energy cost. These metrics were identified and calculated to characterize and quantify the functional performance of the prosthesis.

*1) Load:* Joint loading, joint torque, and GRF are selected to assess the kinematic performance of the prosthesis during STS movement. Particular attention is given to the peak joint loading of the intact side, the joint torque required to perform the movement, and the GRF distribution between the two feet.

*2) Stability:* This section introduces the approach to evaluating stability, which is one of the most important properties of bipedal locomotion [28]. Since the simulation involved in this thesis lasts for 15 seconds, different literature uses various frameworks to define the STS movement with different numbers of phases [29]. This thesis adopts a five-phase framework proposed by Kralj et al. [30] to define the simulation.

Figure 3, which is one stand-up cycle diagram, presents the five consecutive phases related to the STS simulation. Quiet sitting is excluded from the simulation. Since there was no quiet sitting, the simulation started with the initiation phase.

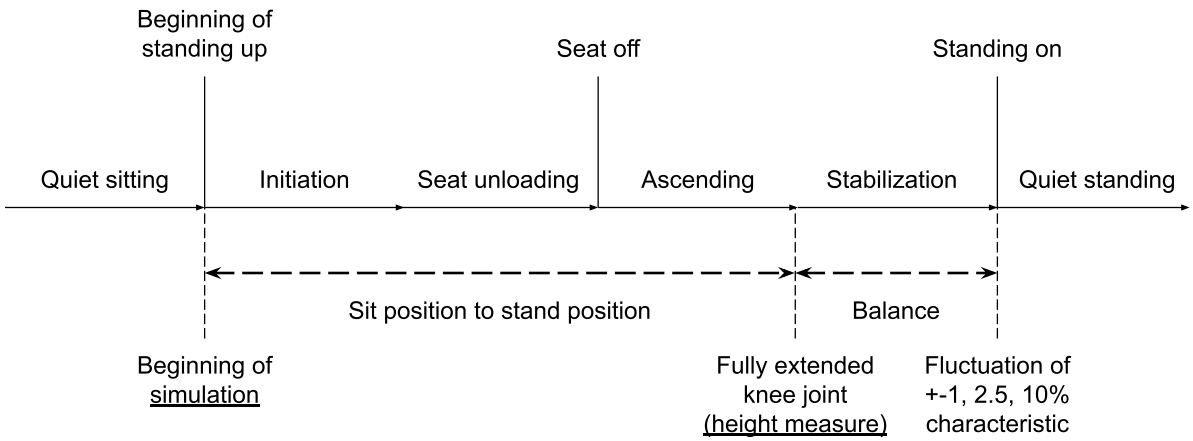


Fig. 3: The cycle diagram of stand-up is presented by Kralj et al. [30]: 5 phases (initiation, seat-unloading, ascending, stabilization, and quiet standing phase) and activities are shown in the upper part of this figure. The bottom part illustrates the 2 phases of the divided simulation, which consists of the sit position to stand position transition phase and the stabilization phase. The marked event of entering the stabilization phase is the fully extended knee joint. When the fluctuation of the ground reaction force is 10% of the stable state, it marks the start of the quiet standing phase.

The simulation is methodically divided into two parts for stability evaluation. The first part is from the sit position to the stand position, which includes initiation, seat unloading, and ascending phases. After the model reaches the standing position, the subsequent stabilization phase starts, which is recognized as the second part of stability evaluation. The quiet standing phase is also excluded. The event markers of the beginning and ending points of the stabilization phase are the knee fully extended and the GRF vertical force being equal to the fluctuation of $10\%$ characteristic of quiet standing. For practical reasons in a prosthesis-involved simulation, the height measure replaced the knee extension. When the height of COM first reaches $0.9\,\mathrm{m}$ (same as the height measure objective function), the model is considered to have reached the stand position and enters the stabilization phase.

This division is based on the selected differing biomechanical stability metrics for the transition phase and stabilization phase, respectively. Firstly, the chosen metric for the transition phase is whole-body angular momentum, where a large angular momentum has been related to a high risk of fall [31]. Another metric for the sequential tuning of the balance phase is the GRF.

*3) Cost of energy:* The cost of energy during the STS movement will be retrieved from the two energy measures of the objective function mentioned previously. These two energy measures aim to evaluate the energy efficiency of the prosthesis performance during the movement.

*4) Kinematics:* To investigate the coordination between the knee and ankle joints during the sit-to-stand movement, the knee angle versus ankle angle of the intact and prosthetic side during the sit-to-stand movement for various prosthetic knee stiffness settings is analyzed. For each stiffness setting, the knee and ankle joint angles were extracted from the simulation data. These angles were plotted against each other to visualize the joint coordination during the STS movement.

### *E. Comparison and Validation*

To validate the simulations, an existing experimental dataset is adopted for comparison. Measured COM pelvis positions in horizontal and vertical directions from one healthy subject's STW movement dataset, which was used by van der Kruk and Geijtenbeek [24] for their study, are compared with the simulation results generated in this thesis. Additionally, only the sit position to the stand position part of the STW dataset is compared with the simulation results1 since the STW dataset starts to walk after the standing position is reached. The comparison of the time-history of the body COM trajectory from experiments with simulations can be a possible validation approach [32]. Other validation approaches, such as comparison with kinematic data [33] and kinetic data [34], are not adopted due to the existence of the prosthetic leg and asymmetric foot placement during STS movement in the simulations.

## III. Results

During the standing-up transition phase, the model first repositions the pelvis while bending the trunk forward. Meanwhile, the intact side leg is also extended to reposition the intact foot position. When the heel strikes the ground, the model initiates seat-off. In this transition phase, the bending trunk recovers to a relatively vertical state, and every other joint's angle reaches a nearly fully extended position. Near the end of the standing-up phase, when the COM of the model reaches a certain height ($0.9\,\mathrm{m}$ in this thesis), the model is considered to have reached a standing position and enters the stabilization phase. During the stabilization phase, the GRF of each foot may fluctuate with the vibration of the upper body.

TABLE I: Optimization Results of Various Prosthetic Knee Stiffness Settings

| File name | Knee stiffness $\mathrm{N\,m\,rad^{-1}}$ | Knee damp $\mathrm{N\,m\,s\,rad^{-1}}$ | Ankle stiffness $\mathrm{N\,m\,rad^{-1}}$ | Ankle damp $\mathrm{N\,m\,s\,rad^{-1}}$ | Cubed muscle stress $(\mathrm{N/m^2})^3$ | Effort J | Total (stress + effort) |
|---|---|---|---|---|---|---|---|
| KS00 | 1.26 | 0.69 | 96.79 | 16.42 | 175.10 | 243.34 | 418.44 |
| KS10 | 10.09 | 0.72 | 82.86 | 13.07 | 172.04 | 256.96 | 429.00 |
| KS20 | 20.34 | 0.5 | 93.61 | 4.98 | 116.05 | 196.98 | 313.03 |
| KS30 | 30.11 | 0.56 | 97.01 | 21.34 | 104.23 | 183.20 | 287.42 |
| KS40 | 39.88 | 4.54 | 88.17 | 8.14 | 108.04 | 189.42 | 297.46 |
| KS50 | 49.82 | 5.04 | 98.25 | 22.03 | 101.43 | 173.93 | 275.36 |
| KS60 | 59.8 | 12.82 | 92.05 | 13.1 | 103.17 | 180.62 | 283.79 |
| KS70 | 70.13 | 21.84 | 93.2 | 18.19 | 118.84 | 186.56 | 305.40 |
| KS80 | 80.09 | 39.1 | 90.7 | 23.18 | 129.17 | 189.26 | 318.45 |
| KS90 | 90.4 | 48 | 85.43 | 6.87 | 177.45 | 205.90 | 383.36 |

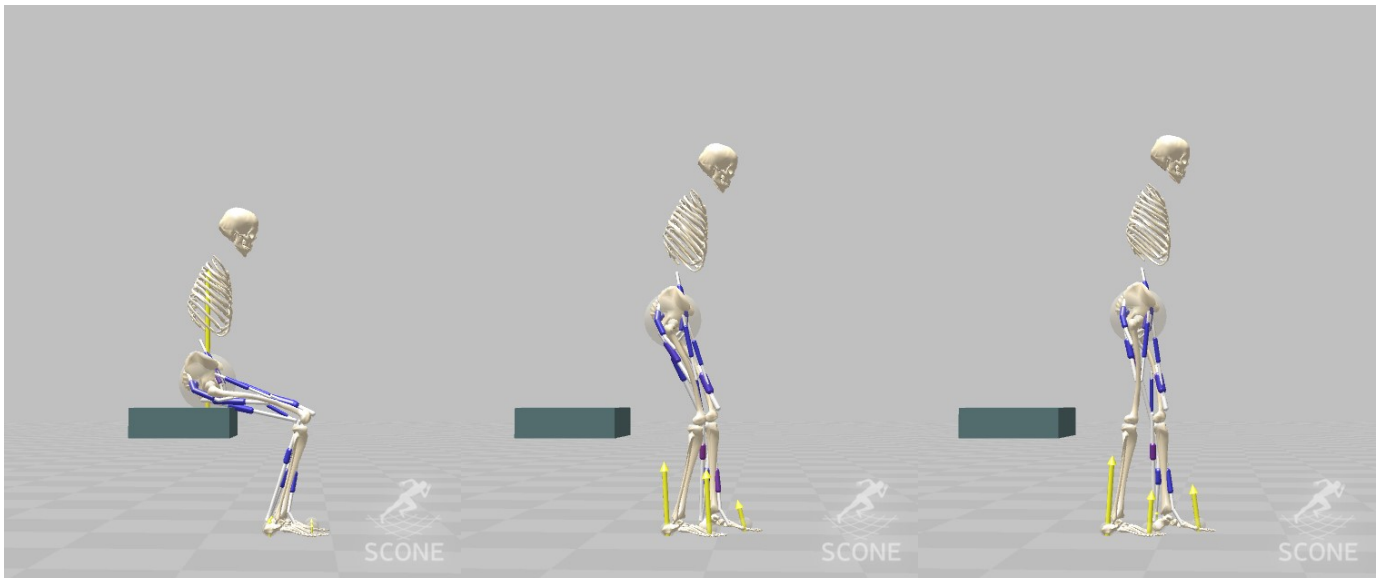


Fig. 4: This figure shows the three mark events of the simulation: 1) initial posture (sit position); 2) stabilization phase starts with the stand position reached; 3) end of the stabilization phase. Additionally, it also shows the re-attached and removed muscles of the right side leg

This phase ends when this fluctuation is within $10\%$ of the mean or expected GRF characteristics. The obtained 10 sets of simulation results, where the optimized model parameters and effort terms are shown in Table I, were analyzed from the following aspects: joint load, stability evaluation, energy cost, and kinematics.

### *A. Joint Load*

This section presents a detailed analysis of joint loads during the sit-to-stand movements across varying prosthetic knee joint stiffness levels. The joint loads for the hip, knee, ankle, and GRF are compared between the intact and prosthetic sides. Results are organized into four groups by joints and GRF, ensuring a comprehensive analysis of the lower body kinematics. Each group includes comparisons between the intact and prosthetic sides. Two plots per group illustrate the peak and average joint loads before and after the stabilization phase starts. Therefore, there are three line charts in each plot.

*1) Hip:* Figure 5 illustrates the variation in joint load dynamics for the hip joint. The plots display both peak and average loads for the intact and prosthetic sides, before and after the stabilization phase begins.

The peak intact side hip load showed a general increasing trend from knee stiffness of $10\,\mathrm{N\,m\,rad^{-1}}$ to $90\,\mathrm{N\,m\,rad^{-1}}$, after the drop from $0\,\mathrm{N\,m\,rad^{-1}}$ to $10\,\mathrm{N\,m\,rad^{-1}}$. Unlike the intact side, the prosthetic side peak hip load shows a maximum at knee stiffness of $50\,\mathrm{N\,m\,rad^{-1}}$. Before reaching the maximum, the hip peak load gradually increases. After the maximum, the prosthetic side peak hip joint load drops but remains at a relatively high level.

The average intact side hip load before the stabilization phase shows a similar tendency to the prosthetic side peak hip load, with a drop at knee stiffness of $10\,\mathrm{N\,m\,rad^{-1}}$ followed by a general increase. However, the average intact side hip load, after the stabilization phase starts, shows a decrease until the knee stiffness reaches $50\,\mathrm{N\,m\,rad^{-1}}$. After the minimum, the intact side average load increases slightly but remains at a relatively low level. For the prosthetic side, the average hip load before the stabilization phase shows a generally increasing trend, though there are two small dips at the stiffness of $20\,\mathrm{N\,m\,rad^{-1}}$ to $60\,\mathrm{N\,m\,rad^{-1}}$. All the average hip loads on the prosthetic side remain at a relatively low level, around 0.3 times the body weight.

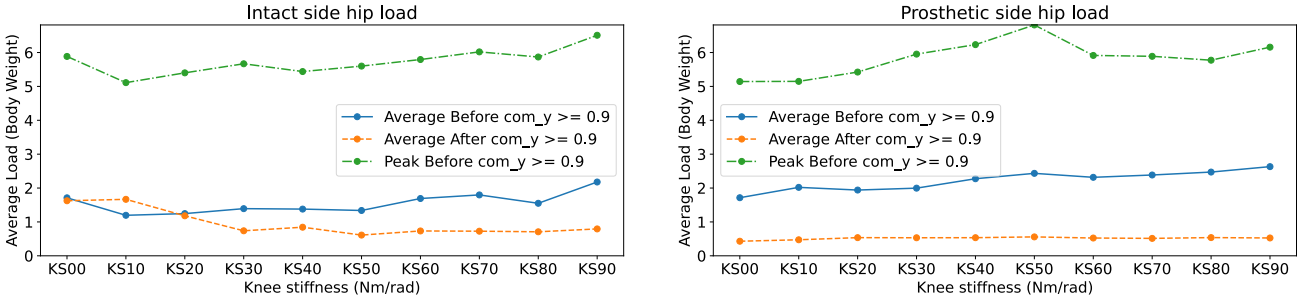


Fig. 5: The line chart illustrates the peak and average loads on the hip joints before and after the stand position is reached. Hip joints exhibit the highest peak load among all the lower extremities. Both average hip loads during standing up show a general increase trend, while, the average hip joint load of the prosthetic side after standing up remains at a relatively low level

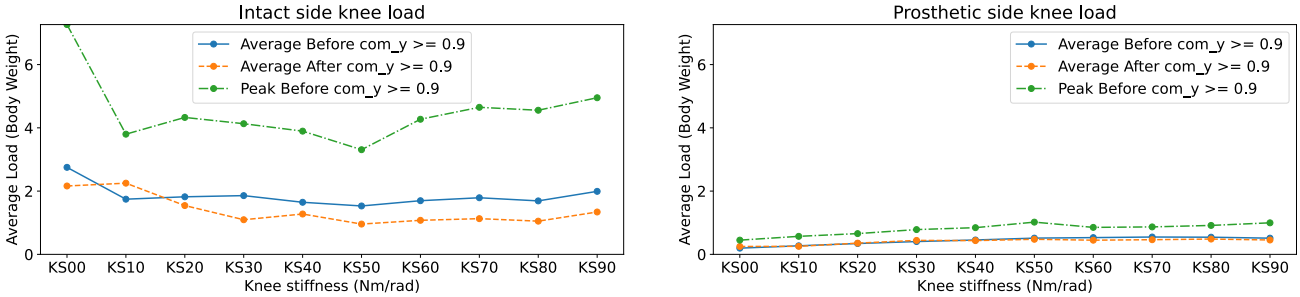


Fig. 6: The line chart illustrates the peak and average loads on the knee joints before and after the stand position is reached. Intact side average knee load increases with the increase of the prosthetic side and reduces with the decrease of the prosthetic side knee load.

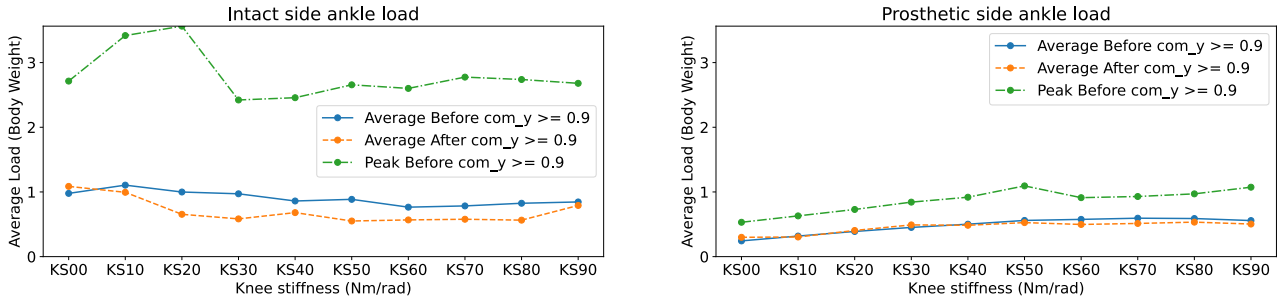


Fig. 7: The line chart illustrates the peak and average loads on the ankle joints before and after the stand position is reached. Intact side average ankle load increases with the increase of the prosthetic side and reduces with the decrease of the prosthetic side ankle load.

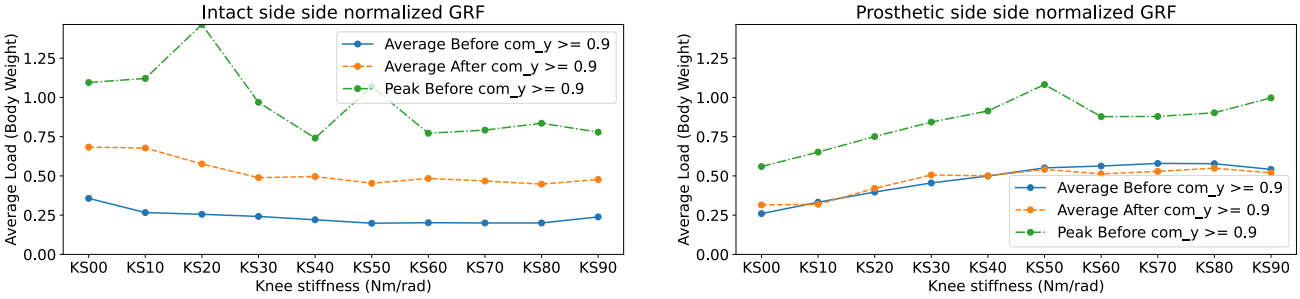


Fig. 8: Line chart illustrating the ground reaction forces (GRF) on the intact and prosthetic sides. Intact side average GRF after standing up increases with the increase of the prosthetic side and reduces with the decrease of the prosthetic side knee load. Meanwhile, the average GRFs generally increase until reaching their maximum and then decrease.

*2) Knee:* Figure 6 illustrates the variation in joint load dynamics for the knee joint. The plots display both peak and average loads for the intact and prosthetic sides, before and after the stabilization phase begins.

The intact side peak knee load shows a dramatic drop at knee stiffness of $10\,\mathrm{N\,m\,rad^{-1}}$. After the drop, the peak load increases at $20\,\mathrm{N\,m\,rad^{-1}}$ and then decreases until it reaches a minimum at $50\,\mathrm{N\,m\,rad^{-1}}$. After this minimum, the knee peak load gradually increases. Differing from the intact side, the knee peak load of the prosthetic side shows a gradual increase across all knee stiffness settings except for a hump at $50\,\mathrm{N\,m\,rad^{-1}}$, which shows a decrease between $50$ and $60\,\mathrm{N\,m\,rad^{-1}}$ followed by an increase afterward.

The average intact side knee load before and after the stabilization phase shows a similar tendency, with a decrease until the minimum at $50\,\mathrm{N\,m\,rad^{-1}}$. Both values increase after the minimum. For the prosthetic side, knee load before and after the stabilization phase shows a similar tendency, where the average load during the stand-up transition phase increases until the maximum is reached at $70\,\mathrm{N\,m\,rad^{-1}}$, followed by a slight decrease. The average load after the stand-up transition phase has a hump and a valley at $30$ and $60\,\mathrm{N\,m\,rad^{-1}}$, respectively.

*3) Ankle:* Figure 7 illustrates the variation in joint load dynamics for the ankle joint. The plots display both peak and average loads for the intact and prosthetic sides, before and after the stabilization phase begins.

The intact side peak ankle load shows a dramatic increase from knee stiffness of $0$ to $20\,\mathrm{N\,m\,rad^{-1}}$ and a significant drop from $20$ to $30\,\mathrm{N\,m\,rad^{-1}}$. After the drop, the peak load increases until $50\,\mathrm{N\,m\,rad^{-1}}$ and then decreases after the valley at $60\,\mathrm{N\,m\,rad^{-1}}$. Unlike the intact side, the prosthetic side peak ankle load shows a similar trend to the prosthetic side peak knee load, where the ankle peak load of the prosthetic side shows a gradual increase across all the knee stiffness settings except for a hump at $50\,\mathrm{N\,m\,rad^{-1}}$.

The average intact side ankle load during the stand-up transition phase reaches a maximum at $10\,\mathrm{N\,m\,rad^{-1}}$, and then decreases to a minimum at $60\,\mathrm{N\,m\,rad^{-1}}$ with a hump at $50\,\mathrm{N\,m\,rad^{-1}}$. After the minimum, the average ankle load increases slightly. After the stabilization phase, the average ankle load first decreases until the knee stiffness is 30 Nm/rad. After a hump at $40\,\mathrm{N\,m\,rad^{-1}}$, the load reaches a minimum and remains at a relatively low level until the knee stiffness is equal to $80\,\mathrm{N\,m\,rad^{-1}}$, with an increase at the end. For the prosthetic side, the average ankle load before and after the stabilization phase shows a similar tendency to the average knee load before and after the stabilization phase.

*4) GRF:* Figure 8 illustrates the variation in GRF dynamics. The plots display both peak and average loads for the intact and prosthetic sides, before and after the stabilization phase begins.

The intact side peak GRF shows three crest values at 20, 50, and $80\,\mathrm{N\,m\,rad^{-1}}$, with the maximum reached at $20\,\mathrm{N\,m\,rad^{-1}}$. Between these crest values, there are two valleys at $40$ (minimum) and $60\,\mathrm{N\,m\,rad^{-1}}$. Unlike the intact side, the prosthetic side peak GRF shows a similar trend to the prosthetic side peak knee and ankle load, where the GRF of the prosthetic side shows a gradual increase across all knee stiffness settings except for a hump at $50\,\mathrm{N\,m\,rad^{-1}}$.

The average intact side GRF during the stand-up transition phase shows a generally decreasing tendency until knee stiffness reaches $80\,\mathrm{N\,m\,rad^{-1}}$, with two humps at $40$ and $60\,\mathrm{N\,m\,rad^{-1}}$. After the stabilization phase, the average GRF first decreases until the knee stiffness is $50\,\mathrm{N\,m\,rad^{-1}}$. After that, the GRF remains at a relatively low level until the knee stiffness reaches $80\,\mathrm{N\,m\,rad^{-1}}$, with an increase at the end. For the prosthetic side, the average GRF before and after the stabilization phase shows a similar tendency to the average knee and ankle load before and after the stabilization phase.

### *B. Stability*

This section presents the findings from the analysis of the whole body angular momentum's peak rate of change among all the prosthetic knee stiffness settings, which is shown in Figure 9. The magnitude of the rate change of the WBAM in the positive direction is always larger than that in the negative direction. According to the line chart in the positive direction, the peak rate of change first increases and reaches the maximum at $20\,\mathrm{N\,m\,rad^{-1}}$. After the maximum, the peak rate of change shows a general decreasing tendency, with a hump at $50\,\mathrm{N\,m\,rad^{-1}}$ and an increased tail at the end.

### *C. Energy*

Figure 10 illustrates the energy consumption metrics during the sit-to-stand movement across various prosthetic knee joint stiffness settings. The data presented includes metabolic energy measures and the summed squared muscle stress.

These two are the objective functions and the metrics to be analyzed. The total effort line shows an initial increase from $0$ to $10\,\mathrm{N\,m\,rad^{-1}}$, reaching a peak at 429, followed by a gradual decrease, and then another rise starting at a stiffness of $50\,\mathrm{N\,m\,rad^{-1}}$, culminating at 383 at the setting of $90\,\mathrm{N\,m\,rad^{-1}}$. The cubed muscle stress line exhibits a downward trend from $0$ to $50\,\mathrm{N\,m\,rad^{-1}}$, stabilizing around the mid-settings, and then a slight increase afterward. The effort line shows a decrease from setting $10$ to $30\,\mathrm{N\,m\,rad^{-1}}$, followed by minor fluctuations, and a rise at higher stiffness settings. The knee damping ratio line remains relatively low and constant across the lower stiffness settings, with a slight increase observed from $40\,\mathrm{N\,m\,rad^{-1}}$ onwards.

### *D. Kinematics*

Figure 11 shows the relationship between knee angle and ankle angle during the sit-to-stand (STS) movement for three prosthetic knee stiffness settings. The knee angle is plotted against the ankle angle for each of the ten predefined stiffness settings, ranging from $20\,\mathrm{N\,m\,rad^{-1}}$ to $80\,\mathrm{N\,m\,rad^{-1}}$ in increments of $30\,\mathrm{N\,m\,rad^{-1}}$. In all cases, the intact side ankle joint exhibits a larger range of motion compared to the prosthetic ankle during the extension of the knee joint. Meanwhile, the range of motion of the prosthetic ankle increases with the increment of prosthetic knee stiffness. At lower stiffness settings ($20\,\mathrm{N\,m\,rad^{-1}}$), the prosthetic ankle shows limited movement,

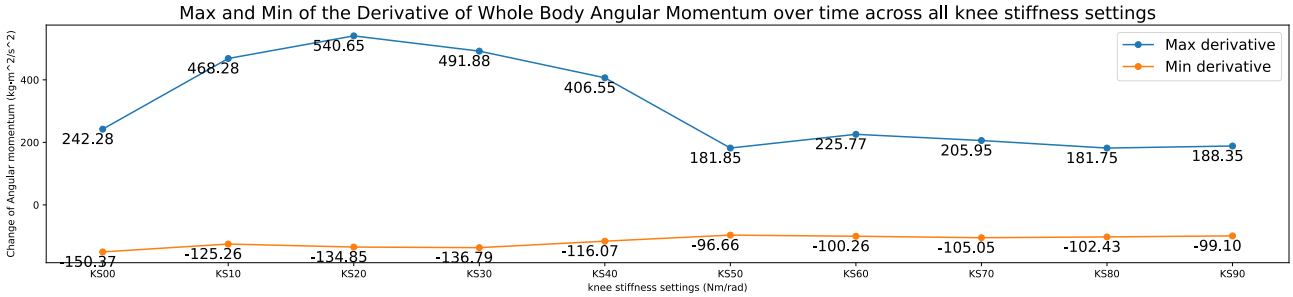


Fig. 9: The line chart shows the peak derivative of Whole-Body Angular Momentum about COM of positive and negative direction in the sagittal plane during STS.

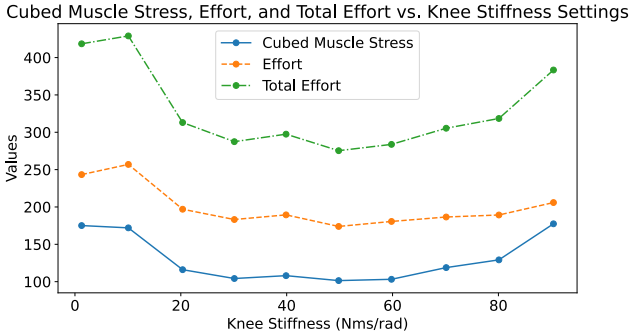


Fig. 10: The line chart illustrates the relationship between knee stiffness settings and three performance metrics: cubed muscle stress (multiplied by 100), effort, and total effort. The knee stiffness settings are varied systematically across ten predefined values. The cubed muscle stress is calculated as the summed squared muscle stress $(\mathrm{N/m^2})^3$ and multiplied by 100 for comparable purposes. Effort is measured in joules, and total effort is the combined metric of energy expenditure.

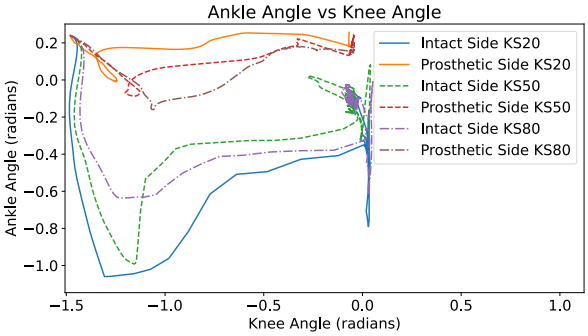


Fig. 11: The plots illustrate the relationship between ankle angle and knee angle during the sit-to-stand (STS) movement for prosthetic knee joint stiffness settings of 20, 50, and $80\,\mathrm{N\,m\,rad^{-1}}$. Each curve shows the angles of the knee and ankle joints, as well as the range of motion and movement patterns of both the intact and prosthetic sides.

whereas at higher stiffness settings (from $50\,\mathrm{N\,m\,rad^{-1}}$), the ankle's range of motion becomes more pronounced. However, the prosthetic side keeps a similar pattern with the increase of the prosthetic knee stiffness.

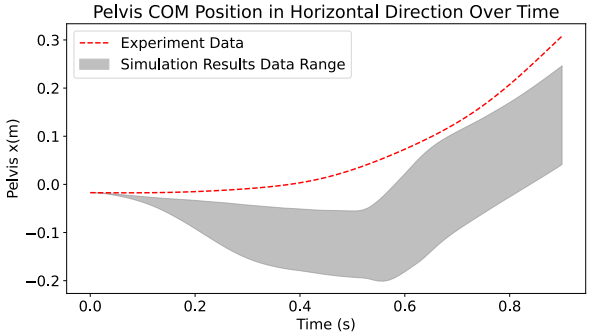


Fig. 12: The diagram shows the comparison of the pelvis's COM position in the horizontal direction between simulation results and the experimental dataset; the grey band is defined by the max and min value of all the simulation results.

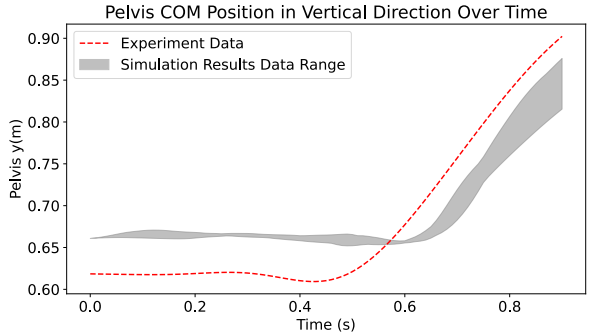


Fig. 13: The diagram shows the comparison of the pelvis's COM position in the vertical direction between simulation results and the experimental dataset; the grey band is defined by the max and min value of all the simulation results.

### *E. Validation*

Figure 12 shows the horizontal position of the pelvis from sit position to stand position (0 - 0.9 s). The grey band represents the range (max and min) of the simulation results, while the solid line depicts the experimental data. The simulation results generally align with the experimental data, capturing the overall trend and key transitional phases. Although the beginning and end of the simulation results have similar tendencies, the middle part of the simulation results shows a generally decreasing movement in the negative direction.

Figure 13 presents the vertical position of the pelvis's COM. Similar to the horizontal position, the grey band indicates the range of simulation results, and the solid line shows the experimental data. The vertical position results demonstrate a close correspondence between the simulated and experimental datasets, particularly during the initial rise after off-chair movement. However, different from the horizontal plot, the starting points of these datasets are different, with a gap of about $0.05\,\mathrm{m}$. Meanwhile, the simulation results' time point of initial rise lags the experimental one by about $0.15\,\mathrm{s}$.

## IV. Discussion

### A. Joint Load

In general, the peak joint loads of the intact side among the simulated prosthetic knee stiffness levels are more irregular than those of the prosthetic side, especially for the knee joint, ankle joint, and GRF. Since the prosthesis consists of two passive joint actuators defined by stiffness and damping ratio in this thesis, the loads are more predictable without the participation of muscle units. This causes the difference between the hip peak load and other prosthetic side loads. The activation of residual muscle units leads to a different shape of the peak hip load line chart. The general increasing tendency of the prosthetic side peak loads indicates that the prosthetic side joint load increases with the increment of knee stiffness, suggesting that high load caused by increasing prosthetic knee stiffness within the socket interaction should be avoided.

Passive actuators are not the only reason why intact side peak loads are more irregular than those of the prosthetic side; other factors such as foot placement, movement strategies, and minor differences in the optimized parameters may also lead to unpredictable intact side peak joint loads. However, some noticeable findings are based on the principle of avoiding relatively high joint peak loading during the standing-up transition phase. For the intact side joints, extremely low or high prosthetic knee stiffness is not preferable, as extreme stiffness may lead to high peak loads.

As for the average joint load, the prosthetic side's average loads of knee, ankle, and GRF before the stabilization phase show a clear tendency that the prosthetic side load increases with the increment of prosthetic knee stiffness until the stiffness reaches $70\,\mathrm{N\,m\,rad^{-1}}$. This suggests that simply increasing the stiffness of the knee joint cannot continuously increase the support from the prosthetic side with a corresponding decrease in the intact side. Due to the exponentially increased prosthetic knee damping ratio, which guarantees a successful STS movement with an increase in prosthetic knee stiffness, the overall load-bearing of the prosthetic actuator does not have a linear relationship with prosthetic knee stiffness. Benefiting the prosthetic side, the intact side average load of knee, ankle, and GRF before the stabilization phase generally decreases with the increase of the prosthetic side before its decrease. Both sides' average hip loads during standing up show an increasing trend with the increment of stiffness.

The average knee, ankle, and GRF joint loads of the prosthetic side, after the stand position is reached, show a similar trend to those during the standing-up phase. However, there are more humps and valleys in the line chart of the average load after the stand position is reached. It is more evident when compared with the intact side, which shows a strategy in terms of load distribution between the intact side and the prosthetic side. During the stabilization phase and quiet standing phase, by shifting the position of COM, redistribution of the joint load can be achieved. Therefore, every hump and valley on the prosthetic side corresponds to a valley or a hump on the intact side. Lastly, benefiting the prosthetic side, the intact side average load of hip, knee, ankle, and GRF after the start of the stabilization phase generally decreases with the increase of the prosthetic side before its decrease.

### B. Stability

The peak rate of change of the WBAM is influenced by the external load, the intact side, and the prosthetic side. In the low prosthetic knee stiffness range (less than or equal to $10\,\mathrm{N\,m\,rad^{-1}}$), the influence on the rate of change of WBAM mainly depends on the intact side. With the increment of prosthetic knee stiffness, the effect of the prosthetic side increases. However, after the prosthetic knee stiffness exceeds $50\,\mathrm{N\,m\,rad^{-1}}$, the presence of the damping ratio begins to reduce the rate of change of WBAM. The reason for these tendencies in both positive and negative directions may be due to the increased damping ratio of the prosthetic knee joint. During the stand-up phase, the increased damping ratio not only decelerates the speed of standing up but also limits the ability to stabilize after standing up.

### C. Energy Cost

The total effort displays a non-linear relationship with knee stiffness, with peaks at lower and higher stiffness settings and a noticeable dip around the mid-range settings. This suggests that, around the mid-range knee stiffness, the prosthetic limb operates more efficiently, reducing the overall energy measure term for the optimization. The minimum total effort observed between $20$ and $80\,\mathrm{N\,m\,rad^{-1}}$ indicates an optimal stiffness range that could be targeted in prosthetic design to enhance energy efficiency under similar simulation conditions.

The cubed muscle stress shows a similar trend to the effort measure. The pattern implies that increasing stiffness up to a certain point reduces muscle stress or effort, likely because the support and mechanism provided by the prosthetic limb are closer to that of the intact side, where extra effort is not required for control and balance. However, the slight increase in muscle stress at the highest stiffness settings suggests that an overly stiff prosthesis with a high damping ratio may introduce inefficiencies to the STS maneuver.

The observed trends in knee damping and effort further support the need for optimized stiffness with a certain damping ratio. The gradual rise in knee damping energy dissipation at higher stiffness settings highlights the increased mechanical work required to stabilize and achieve the STS movement. The optimal range for minimal effort reinforces the importance of fine-tuning prosthetic stiffness to improve the energy efficiency of the prosthesis.

### D. Kinematics

In high prosthetic knee stiffness settings, the kinematic results indicate an increased contribution of the prosthetic side during the STS movement, as evidenced by the larger range of motion in the prosthetic side ankle joint. This suggests that a larger external load is applied to the prosthetic side with the increment of the prosthetic knee stiffness. Additionally, the pattern of the intact side shows a consistent and similar strategy applied across all simulations. There is a constrained tendency for the prosthetic side pattern to become closer to the intact side.

### E. Validation

The simulation results demonstrate a strong correspondence with the experimental data, as indicated by the grey band in Figure 12. The overall trend and the change in horizontal position between sit position and stand position were effectively captured by the simulations. However, during the first $0.6\,\mathrm{s}$, the grey band simulation results show a backward movement of the pelvis's COM. This behavior is often coupled with exaggerated trunk flexion, which is a widely reported STS strategy [35]–[37]. The relatively large movement between the contact model of the buttocks and the contact model of the chair is not expected. Specifically, the sphere contact model can rotate on the box contact model. Therefore, extra constraints and a non-sphere contact model are required for better modeling the interaction and limiting the relative displacement between the buttocks and the chair.

In the vertical direction, the alignment between the simulated and experimental vertical COM positions, shown in Figure 13, underscores the robustness of the simulation model in replicating the upward movement. The minor discrepancies near the start of the movement may be attributed to the chair height difference in the model and the experimental setup. The plot also shows that the simulation results' rising time lags behind the experimental dataset by about $0.2\,\mathrm{s}$. This may potentially be because the experimental data was conducted by a healthy subject.

The alignment with experimental data reinforces the model's feasibility in optimizing prosthetic parameters. However, the observed discrepancies also point to the need for ongoing refinement in constraints, model setups, and validation against diverse datasets related to prosthesis users to ensure the model's generalizability and accuracy. The validation of the simulation results against experimental data provides a certain foundation for the continued development and application of predictive simulation models in prosthetic parameter optimization.

### F. Limitations

*1) 2D Constraints:* One of the constraints and assumptions of the model is that all the joints are adjusted and only rotated or translated in the sagittal plane, which means side falls are excluded from the simulations and falls only happen in the sagittal plane. Other forces or moments that may potentially cause a rotation or a lean in the frontal plane are eliminated due to the existence of 2D constraints. For example, due to the asymmetry caused by the prosthesis, it is difficult for both legs to perform symmetric behavior, and subsequent resultant moments from the lower extremities may generate a rotation. However, 2D constraints would artificially compensate for these extra forces and moments to prevent the model from rotating in the frontal plane.

*2) Muscle Units:* Raveendranathan et al. mentioned that the eight muscles on the prosthetic side's transected femur are disabled during their performed simulations since these muscles' contribution to STS is unknown due to a lack of clinical evidence in the literature and a lack of detailed physical information [16]. The adjustment of the respective muscles should refer to anatomical information and experimental support. Therefore, one possible solution for these muscles is to model them as equivalent joint motors that provide force or moment according to the state of the joint with the cooperation of a controller.

*3) Local Optimum:* Although the intervals and thresholds of some SCONE measure terms are set to become zero at a certain stage so that only the effort terms will be the remaining term to be optimized, however, it is inevitable to have a local optimum result at the end of the optimization due to the redundancy of the musculoskeletal system and the optimization of over five hundred parameters. Different sets of controller parameters can lead to similar task movements, and trade-offs between the remaining effort measure terms may lead to similar scores but different kinematic or kinetic data. To prevent various or arbitrary results with large fluctuations, one possible solution is to have a more detailed set of measure terms.

*4) Socket Interaction:* The interaction between the socket and the residual limb is not taken into consideration in this thesis, as it is not the focus of this research. Currently, the prosthesis is based on the modification of one of the legs by deleting and re-attaching muscles and adding extra joint actuators that behave like prosthetic devices.

*5) Joint Motor:* The current prosthesis is defined as a joint motor actuator, which is a passive device with a stiffness and damping ratio. However, in practice, friction force cannot be negligible during the rotation motion of the joint. Apart from passive prostheses, there are also semi-active and active prostheses available for modeling and implementation. The adjusted controllers in SCONE may potentially be suitable for active prostheses.

*6) Methodological Limitations:* The approach of generating data is also debatable in this thesis. By setting a threshold, all the measures become zero below the respective threshold in the end, except for the effort terms. However, there is no clear literature supporting setting a proper threshold, and the performance of these measures cannot be reflected in the measure score since they become zero as long as they are below the threshold. These differences in performance potentially caused the optimization variation, and according to the data analysis, they showed a certain amount of uncertainty in the kinematic and kinetic plots.

*7) Theoretical Limitations:* The controllers adopted in this model were initially from the STW simulations and designed

for an intact model rather than a prosthetic model. Three reflex controllers are implemented in the prosthetic model, two are expected to control standing up, and the last one aims for balance control. Although part of the feedback control loops have been removed from the original controller to make the controllers work in the new model, it is unclear whether the structures of the control loop have been changed or the control strategies have been altered.

*8) Practical Limitations:* Since the musculoskeletal model and the controllers have redundancies, there are multiple local optima, which are all potential solutions to the predictive simulation. Meanwhile, the final optimization solution is highly dependent on the initial guess, which is a parameter file that includes all the parameters for optimization. To maintain consistency, the strategy of this simulation is to use the same initial guess and try to keep the result with the same STS strategy. This strategy leads to the motion having the same behavior where the intact leg will always step forward first before standing up, as previously mentioned in the results section. This limitation eliminates the possibility of acquiring other potential motions that may have better performance. For example, some of the optimization results with lower prosthetic knee stiffness show a new strategy where the intact leg steps backward first during standing up. For consistency, this is not included in the analysis, but it shows that different prosthesis conditions may require different suitable movements to achieve better performance.

Another issue during optimization is that there are some sliding motions between the feet and the ground for all the optimization results. This may potentially be because the three reflex controllers' parameters are not well optimized, leading to undesired muscle activation during the quiet standing phase. More measures, such as penalizing the sliding feet, may solve such issues. Another solution could be to replace the third reflex controller with a well-designed balance controller for the quiet standing phase.

### G. Future Work and Recommendation

*1) From 2D to 3D:* A more comprehensive 3D model can be further developed based on this 2D model, requiring adjustments in the aspects of the model, controllers, and measures. Firstly, the model needs to add more degrees of freedom to support movement or rotation in the frontal plane, and more muscle units should be added or minor adjustments made to some joints' range of motion if needed. Secondly, controllers may need complex feedback from the new muscles or new degrees of freedom, especially in terms of preventing side falls. Thirdly, when conducting the simulations in SCONE, more objective functions or measures should be added to achieve acceptable movement and balance in the frontal plane. The 3D model will provide the possibility of falling sideways, which leads to the evaluation of a more comprehensive symmetry of movements.

*2) Customized Model:* The model can be further customized according to the subjects in biomechanical experiments or patients for clinical applications. The former could use the customized model to conduct inverse kinetics and inverse dynamics through OpenSim to obtain kinematic and kinetic data from experiments. For example, motion capture data can be used with a lower limb prosthetic model to conduct inverse kinetic simulations. The latter could utilize OpenSim and SCONE to create patient-specific prosthetic models and disease-oriented controllers. For example, the variation in the length of the residual limb between prosthetic users may lead to different movement strategies. Meanwhile, the amount of muscle in the residual limb also influences the muscle units' parameters and the attachment point in the model, which potentially defines the upper limit torque generated from the residual hip joint during simulations. Lastly, the prosthetic joints in this model are represented as passive devices with specified stiffness and damping ratios, but without braking (friction force). Therefore, future research could explore active, semi-active, and alternative passive prostheses.

*3) Socket Interaction:* The interaction between the residual limb and the prosthetic socket could also be an area of interest for research. The interaction here does not refer to FEM but to more precise modeling in the musculoskeletal system simulations. It may potentially be modeled as a customized joint in the model, where the limb-socket joint should allow limited translations and rotations during movement. The precision of modeling would be highly dependent on the context of the simulations and research interest.

*4) Other Movements:* Only the sit-to-stand transition and quiet standing were simulated in this thesis. Other ADLs should also be simulated and optimized. Firstly, the transition from the stand position to the sit position can be further optimized as an extension of this thesis to complete the sit-to-stand-to-sit cycle. The strategy and lack of feedback during the stand-to-sit movement make it different from the sit-to-stand transition. Additionally, residual limb muscle modeling and exploring other determinants of the sit-to-stand (STS) task, such as sit-to-walk, can be valuable extensions of this research.

*5) Contact Model:* The simulation results and validation results show that the pelvis in the simulation exhibits excessive mobility compared to the experimental data, particularly evident in the horizontal rolling of the spherical contact model of the buttocks. Therefore, to limit excessive movement, feasible approaches include adjusting the friction coefficient, changing the shape of the buttocks, or penalizing the rolling behavior during the optimization process.

*6) Prosthetic Joint Actuators:* In this simulation, the joint motor actuator in Hyfydy is chosen to represent the passive prosthetic joint actuator. However, some elements are missing in the joint motor, such as the brake and pre-stiffness. In this simulation, the joint motor does not provide any torque at rest length with zero velocity, which is unexpected during quiet standing. Therefore, it is recommended to include more actuators in Hyfydy. Additionally, when converting the OpenSim model to the Hyfydy model, it would be beneficial to ensure compatibility with the various actuators available in OpenSim.

## V. Conclusion

The prosthetic side exhibited a general increase in both peak and average joint load with the increasing prosthetic knee

stiffness settings during and after the standing-up transition phase, although the average joint load decreased after the stiffness setting of $70\,\mathrm{N\,m\,rad^{-1}}$ with the damping ratio of $22\,\mathrm{N\,m\,s\,rad^{-1}}$. This implied the continuous contribution of the prostheses with increments of prosthetic knee stiffness within a certain range. Extremely high prosthetic knee stiffness required high damping ratios, potentially leading to a negative contribution to the STS movement. Peak loads of the intact side were notably higher at extreme stiffness settings for most cases, influenced by foot placement, movement strategies, and the compensatory actions required to maintain balance, suggesting a need to avoid overly high stiffness to prevent excessive joint load.

Whole-body angular momentum's rate of change peak values during STS movement indicates that relatively high prosthetic knee stiffness had a better dynamic stability performance. Energy consumption showed a non-linear relationship with knee stiffness. The optimal stiffness settings (between 20 and $80\,\mathrm{N\,m\,rad^{-1}}$) were identified. The kinematics of the knee and ankle joint imply that relatively high knee stiffness potentially leads to more prosthetic contributions. Validation in the vertical direction showed a strong correspondence with an offset, which was caused by the difference in the chair height in the experimental setup and modeling, while the horizontal direction showed the defect of modeling the buttocks as a sphere.

The findings of this study demonstrated the potential of predictive simulation for the design and customization of prosthetic knees. However, the approach adopted in this study is still limited by the model (degrees of freedom, muscle units, joint motor, and socket interaction), STS strategy (exaggerated trunk flexion), and simulation-related limitations.

Therefore, several areas still need further investigation: Developing more complex 3D models that include additional degrees of freedom, adjusted contact models, and prosthetic joint actuators will enhance the accuracy and applicability of the findings. Investigating the interaction between the residual limb and the prosthetic socket will provide insights into improving optimization. Extending the analysis to other activities of daily living, such as standing-to-sitting or gait, will offer a more comprehensive view of improving prosthetic performance.

## Data Availability Statement

The simulation code and results related to this study are available in the corresponding GitHub repository [38].

## References


[1] P. Riley, D. Krebs, and R. Popat, "Biomechanical analysis of failed sit-to-stand," vol. 5, no. 4, pp. 353–359.

[2] M. J. Highsmith, J. T. Kahle, S. L. Carey, D. J. Lura, R. V. Dubey, K. R. Csavina, and W. S. Quillen, "Kinetic asymmetry in transfemoral amputees while performing sit to stand and stand to sit movements," *Gait & posture*, vol. 34, no. 1, pp. 86–91, 2011.

[3] T. Everett and C. Kell, *Human movement: An introductory text*. Elsevier health sciences, 2010.

[4] H. Burger, J. Kuželički, and Č. Marinček, "Transition from sitting to standing after trans-femoral amputation," *Prosthetics and orthotics international*, vol. 29, no. 2, pp. 139–151, 2005.

[5] S. K. Au and H. M. Herr, "Powered ankle-foot prosthesis," *IEEE Robotics & Automation Magazine*, vol. 15, no. 3, pp. 52–59, 2008.

[6] A. F. Azocar, L. M. Mooney, L. J. Hargrove, and E. J. Rouse, "Design and characterization of an open-source robotic leg prosthesis," in *2018 7th IEEE International Conference on Biomedical Robotics and Biomechatronics (Biorob)*. IEEE, 2018, pp. 111–118.

[7] W. C. Miller, M. Speechley, and B. Deathe, "The prevalence and risk factors of falling and fear of falling among lower extremity amputees," *Archives of physical medicine and rehabilitation*, vol. 82, no. 8, pp. 1031–1037, 2001.

[8] W. Liang, Z. Qian, W. Chen, H. Song, Y. Cao, G. Wei, L. Ren, K. Wang, and L. Ren, "Mechanisms and component design of prosthetic knees: A review from a biomechanical function perspective," vol. 10.

[9] R. Ito, Y. Oppata, M. Katsumura, K. Yano, Y. Kobayashi, and H. Krebs, "Robotic knee orthosis to prevent falling during a standing up assistance," pp. 1556–1559.

[10] D. A. Winter, *Biomechanics and motor control of human movement*. John wiley & sons, 2009.

[11] N. P. Fey, G. K. Klute, and R. R. Neptune, "Optimization of prosthetic foot stiffness to reduce metabolic cost and intact knee loading during below-knee amputee walking: a theoretical study," 2012.

[12] M. A. Price, P. Beckerle, and F. C. Sup, "Design optimization in lower limb prostheses: A review," *IEEE Transactions on Neural Systems and Rehabilitation Engineering*, vol. 27, no. 8, pp. 1574–1588, 2019.

[13] S. Pejhan, F. Farahmand, and M. Parnianpour, "Design optimization of an above-knee prosthesis based on the kinematics of gait," in *2008 30th Annual International Conference of the IEEE Engineering in Medicine and Biology Society*. IEEE, 2008, pp. 4274–4277.

[14] J. Camargo, K. Bhakta, J. Maldonado-Contreras, S. Zhou, K. Herrin, and A. Young, "Opensim model for biomechanical analysis with the open-source bionic leg," in *2022 International Symposium on Medical Robotics (ISMR)*. IEEE, 2022, pp. 1–6.

[15] R. Carloni, R. Luinge, and V. Raveendranathan, "The gait1415+ 2 opensim musculoskeletal model of transfemoral amputees with a generic bone-anchored prosthesis," *Medical Engineering & Physics*, vol. 123, p. 104091, 2024.

[16] V. Raveendranathan, V. G. Kooiman, and R. Carloni, "Musculoskeletal model of osseointegrated transfemoral amputees in opensim," *Plos one*, vol. 18, no. 9, p. e0288864, 2023.

[17] M. Grimmer and A. Seyfarth, "Stiffness adjustment of a series elastic actuator in a knee prosthesis for walking and running: The trade-off between energy and peak power optimization," in *2011 IEEE/RSJ International Conference on Intelligent Robots and Systems*, 2011, pp. 1811–1816.

[18] Y. S. Narang, V. Murthy Arelekatti, and A. G. Winter, "The effects of the inertial properties of above-knee prostheses on optimal stiffness, damping, and engagement parameters of passive prosthetic knees," *Journal of Biomechanical Engineering*, vol. 138, no. 12, p. 121002, 2016.

[19] S. L. Delp, F. C. Anderson, A. S. Arnold, P. Loan, A. Habib, C. T. John, E. Guendelman, and D. G. Thelen, "Opensim: open-source software to create and analyze dynamic simulations of movement," *IEEE transactions on biomedical engineering*, vol. 54, no. 11, pp. 1940–1950, 2007.

[20] C. L. Dembia, N. A. Bianco, A. Falisse, J. L. Hicks, and S. L. Delp, "Opensim moco: Musculoskeletal optimal control," *PLOS Computational Biology*, vol. 16, no. 12, p. e1008493, 2020.

[21] T. Geijtenbeek, "Scone: Open source software for predictive simulation of biological motion," *Journal of Open Source Software*.

[22] ——, "The Hyfydy simulation software," 11 2021, https://hyfydy.com. [Online]. Available: https://hyfydy.com

[23] A. Kewley, J. Beesel, and A. Seth, "Opensim creator (0.5.12)," 2024. [Online]. Available: https://doi.org/10.5281/zenodo.11086325

[24] E. van der Kruk and T. Geijtenbeek, "A planar neuromuscular controller to simulate age-related adaptation strategies in the sit-to-walk movement." 2023.

[25] K. H. Hunt and F. R. E. Crossley, "Coefficient of restitution interpreted as damping in vibroimpact," vol. 42, no. 2, pp. 440–445, 1975, publisher: American Society of Mechanical Engineers Digital Collection.

[26] M. Millard, T. Uchida, A. Seth, and S. L. Delp, "Flexing computational muscle: modeling and simulation of musculotendon dynamics," *Journal of biomechanical engineering*, vol. 135, no. 2, p. 021005, 2013.

[27] J. M. Wang, S. R. Hamner, S. L. Delp, and V. Koltun, "Optimizing locomotion controllers using biologically-based actuators and objectives," *ACM Transactions on Graphics (TOG)*, vol. 31, no. 4, pp. 1–11, 2012.

[28] K. Mombaur, H. Vallery, Y. Hu, J. Buchli, P. Bhounsule, T. Boaventura, P. M. Wensing, S. Revzen, A. D. Ames, I. Poulakakis *et al.*, "Control of motion and compliance," *Bioinspired Legged Locomotion*, pp. 135–346, 2017.

[29] M. Galli, V. Cimolin, M. Crivellini, and I. Campanini, "Quantitative analysis of sit to stand movement: Experimental set-up definition and application to healthy and hemiplegic adults," vol. 28, no. 1, pp. 80–85.

[30] A. Kralj, R. Jaeger, and M. Munih, "Analysis of standing up and sitting down in humans: Definitions and normative data presentation," vol. 23, no. 11, pp. 1123–1138, 1990.

[31] A. Silverman and R. Neptune, "Differences in whole-body angular momentum between below-knee amputees and non-amputees across walking speeds," *Journal of Biomechanics*, vol. 44, no. 3, pp. 379–385, 2011.

[32] S. Bajelan and M. R. Azghani, "Musculoskeletal modeling and simulation of three various sit-to-stand strategies: An evaluation of the biomechanical effects of the chair-rise strategy modification," *Technology and Health Care*, vol. 22, no. 4, pp. 627–644, 2014.

[33] Y. R. Mao, X. Q. Wu, J. L. Zhao, W. L. A. Lo, L. Chen, M. H. Ding, Z. Q. Xu, R. H. Bian, D. F. Huang, and L. Li, "The crucial changes of sit-to-stand phases in subacute stroke survivors identified by movement decomposition analysis," *Frontiers in Neurology*, vol. 9, p. 185, 2018.

[34] M. K. Mak, O. Levin, J. Mizrahi, and C. W. Hui-Chan, "Joint torques during sit-to-stand in healthy subjects and people with parkinsonâs disease," *Clinical Biomechanics*, vol. 18, no. 3, pp. 197–206, 2003.

[35] D. M. Scarborough, C. A. McGibbon, and D. E. Krebs, "Chair rise strategies in older adults with functional limitations." *Journal of Rehabilitation Research & Development*, vol. 44, no. 1, 2007.

[36] E. van der Kruk and T. Geijtenbeek, "Increased trunk flexion in standing up is related to muscle weakness rather than pain avoidance in individuals with unilateral knee pain; a simulation study." *medRxiv*, pp. 2023–12, 2023.

[37] E. van Der Kruk, A. K. Silverman, P. Reilly, and A. M. Bull, "Compensation due to age-related decline in sit-to-stand and sit-to-walk," *Journal of biomechanics*, vol. 122, p. 110411, 2021.

[38] Y. Li, "Predictive-simulation-of-prosthetic-model-during-sit-to-stand," 2024. [Online]. Available: https://github.com/mandarin12302/Predictive-simulation-of-prosthetic-model-during-sit-to-stand

## APPENDIX

### A. Lumbar and Thorax

Figure 14 illustrates the variation in lumbar joint load and thorax joint load dynamics. The plots display both peak and average loads, before and after the stabilization phase begins.

The peak lumbar joint load first decreases and reaches its minimum at $20\,\mathrm{N\,m\,rad^{-1}}$, then increases to a maximum at $40\,\mathrm{N\,m\,rad^{-1}}$. After the maximum, the value decreases until $70\,\mathrm{N\,m\,rad^{-1}}$ and increases afterward. The average lumbar joint load before and after stabilization starts remains at a similar level.

The peak thorax joint load first increases until the knee stiffness reaches $30\,\mathrm{N\,m\,rad^{-1}}$, then decreases until $70\,\mathrm{N\,m\,rad^{-1}}$. After the decrease, the value increases until the end. The average thorax joint load before and after stabilization starts remains at a similar level.

Therefore, in the lumbar and thorax joints, the peak loads do not show a clear trend. However, the average loads of these two joints before and after stabilization show an increase when the prosthetic knee stiffness is near the extreme values (0 and $90\,\mathrm{N\,m\,rad^{-1}}$ in this simulation).

### B. Whole Body Angular Momentum

This section presents the findings from the analysis of whole-body angular momentum during the sit-to-stand movement. The peak whole-body angular momentum among all the prosthetic knee stiffness settings is shown in Figure 15. The magnitude of the WBAM in the negative direction is larger than that in the positive direction at the same prosthetic knee stiffness, except for the knee stiffness of $90\,\mathrm{N\,m\,rad^{-1}}$. Therefore, the magnitude of the peak WBAM keeps decreasing from 10 to $80\,\mathrm{N\,m\,rad^{-1}}$, and increases at the stiffness of 0 and $90\,\mathrm{N\,m\,rad^{-1}}$.

The magnitude in the positive direction shows an increasing trend after $10\,\mathrm{N\,m\,rad^{-1}}$, while the magnitude in the negative direction shows a decreasing tendency after $10\,\mathrm{N\,m\,rad^{-1}}$. Referring to the movement of STS, it can be found that the positive peak occurs after the standing-up movement, while the negative peak occurs during the standing-up transition phase.

### C. Stabilization Duration Analysis Based on GRF

Figure 16 shows the duration of the stabilization phase across all the stiffness settings based on the measure of the intact side and prosthetic side GRF. The line chart does not show a clear trend of how stabilization duration changes with the increment of prosthetic knee stiffness. The observed zigzag pattern indicates rapid and repetitive changes in the stabilization duration with an increment of stiffness. The maximum duration and the minimum occur at knee stiffness of 20 and $50\,\mathrm{N\,m\,rad^{-1}}$, respectively.

### D. Kinematics

Figure 11 shows all the plots of knee angle versus ankle angle during the sit-to-stand (STS) movement for all the prosthetic knee stiffness settings within the simulations. The knee angle is plotted against the ankle angle for each of the ten predefined stiffness settings, ranging from $0\,\mathrm{N\,m\,rad^{-1}}$ to $90\,\mathrm{N\,m\,rad^{-1}}$ in increments of $10\,\mathrm{N\,m\,rad^{-1}}$. In all cases, the intact side ankle joint exhibits a larger range of motion compared to the prosthetic ankle during the extension of the knee joint. Meanwhile, the range of motion of the prosthetic ankle increases with the increment of prosthetic knee stiffness. At lower stiffness settings (below $30\,\mathrm{N\,m\,rad^{-1}}$), the prosthetic ankle shows limited movement, whereas at higher stiffness settings (from $60\,\mathrm{N\,m\,rad^{-1}}$), the ankle's range of motion becomes more pronounced. However, the prosthetic side keeps a similar pattern with the increase of the prosthetic knee stiffness.

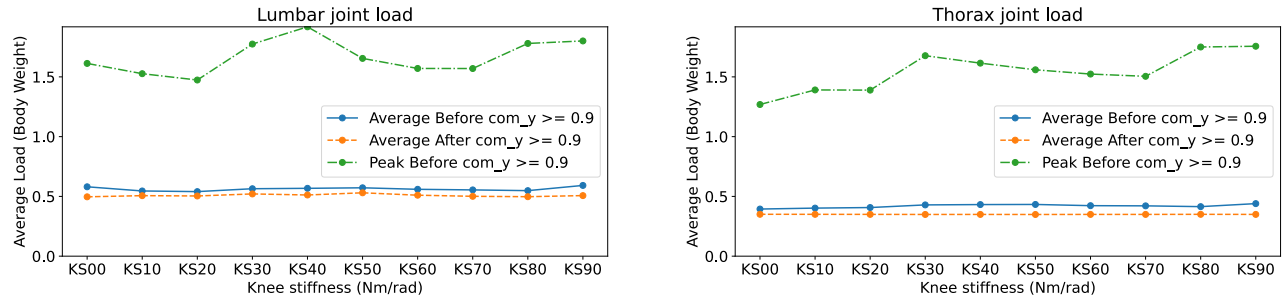


Fig. 14: Line chart illustrating the peak and average loads on the lumbar and thorax joints before and after the stand position is reached. Each plot includes three lines representing the peak value before the stand position is reached, the average value before the stand position is reached, and the average value after the stand position is reached. The knee stiffness settings (in Nm/rad) are varied systematically across ten predefined values.

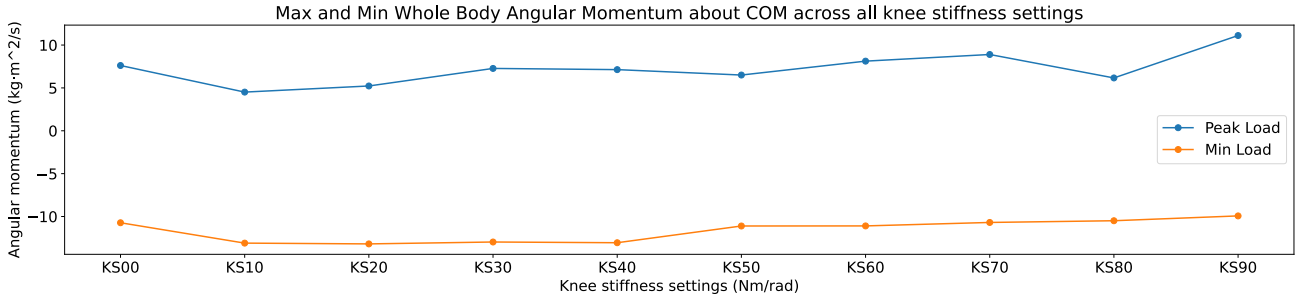


Fig. 15: The line chart shows the peak Whole-Body Angular Momentum about COM of positive and negative direction in the sagittal plane during STS.

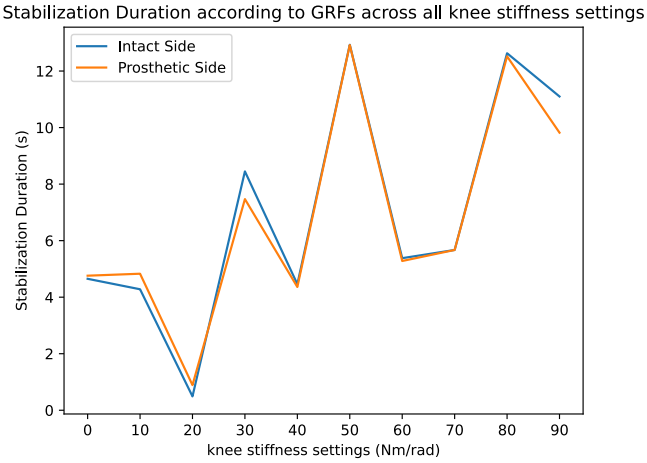


Fig. 16: The line chart of the time duration of the stabilization phase across all the knee stiffness settings in the intact and prosthetic sides. The time duration is identified based on the fluctuation of the GRFs.

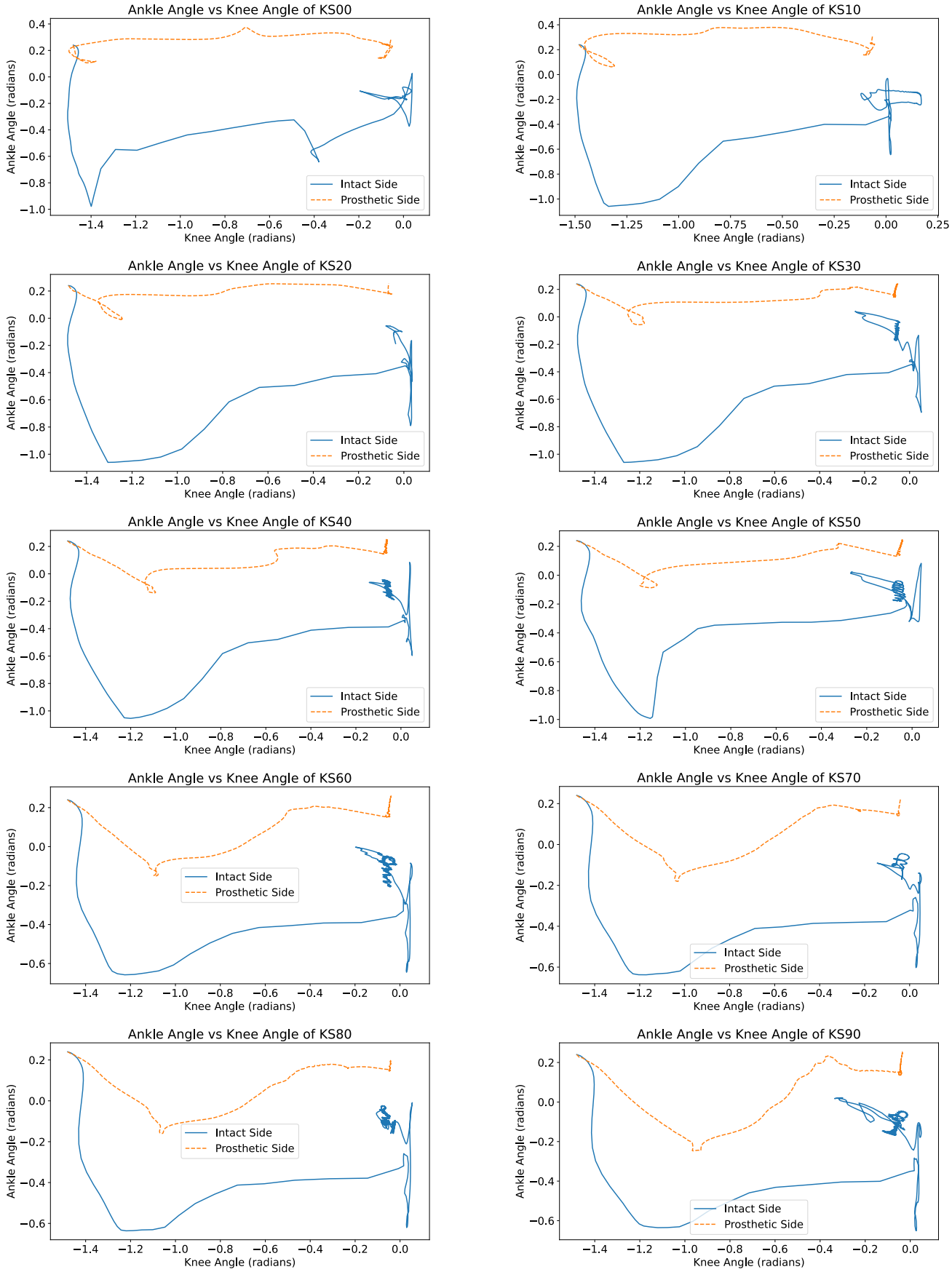


Fig. 17: Knee angle vs. ankle angle for varying knee stiffness settings from 0 to 90 Nm/rad. Each subplot represents a different knee stiffness setting.